catalysts

MDPI

Article

Niobium Oxide Catalysts as Emerging Material for Textile Wastewater Reuse: Photocatalytic Decolorization of Azo Dyes

Alexsandro Jhones dos Santos [1], Luana Márcia Bezerra Batista [2], Carlos Alberto Martínez-Huitle [1,*], Ana Paula de Melo Alves [3,*] and Sergi Garcia-Segura [4,*]

1 Laboratório de Eletroquímica Ambiental e Aplicada (LEAA), Institute of Chemistry, Federal University of Rio Grande do Norte, Lagoa Nova, 59078-970 Natal, Brazil; alexsandrojhones@hotmail.com
2 Instituto Federal de Pernambuco, Campus Afogados da Ingazeira, Rua Edson Barbosa de Araújo, s/n, Bairro Manoela Valadares, 56800-000 Afogados da Ingazeira-PE, Brazil; luanamarciaufrn@gmail.com
3 Laboratório de Combustíveis e Materiais (LACOM), Department of Chemistry, Federal University of Paraíba, Campus I—Lot. Cidade Universitária, 58051-900 João Pessoa, Brazil
4 Nanosystems Engineering Research Center for Nanotechnology-Enabled Water Treatment, School of Sustainable Engineering and the Built Environment, Arizona State University, Tempe, AZ 85287-3005, USA
* Correspondence: carlosmh@quimica.ufrn.br (C.A.M.-H.); anachemistry@pq.cnpq.br (A.P.d.M.A.); sergio.garcia.segura@asu.edu (S.G.-S.)

Received: 2 December 2019; Accepted: 12 December 2019; Published: 14 December 2019

Abstract: Niobium-based metal oxides are emerging semiconductor materials with barely explored properties for photocatalytic wastewater remediation. Brazil possesses the greatest reserves of niobium worldwide, being a natural resource that is barely exploited. Environmental applications of solar active niobium photocatalysts can provide opportunities in the developing areas of Northeast Brazil, which receives over 22 MJ m^2 of natural sunlight irradiation annually. The application of photocatalytic treatment could incentivize water reuse practices in small and mid-sized textile businesses in the region. This work reports the facile synthesis of Nb_2O_5 catalysts and explores their performance for the treatment of colored azo dye effluents. The high photoactivity of this alternative photocatalyst makes it possible to quickly obtain complete decolorization, in less than 40 min of treatment. The optimal operational conditions are defined as 1.0 g L^{-1} Nb_2O_5 loading in slurry, 0.2 M of H_2O_2, pH 5.0 to treat up to 15 mg L^{-1} of methyl orange solution. To evaluate reutilization without photocatalytic activity loss, the Nb_2O_5 was recovered after the experience and reused, showing the same decolorization rate after several cycles. Therefore, Nb_2O_5 appears to be a promising photocatalytic material with potential applicability in wastewater treatment due to its innocuous character and high stability.

Keywords: advanced oxidation processes; azo dye; sustainable resources; niobium; water reuse; water treatment

1. Introduction

New trends in photocatalysis aim to identify niche applications for emerging semiconductor materials within a sustainable context. Titanium dioxide is the most studied photocatalyst and photoelectrocatalyst for water treatment [1,2] and water splitting applications [3,4]. However, recent research efforts have explored alternative semiconductor materials to overcome the most stringent barrier for the implementation of TiO_2 in developing countries: its low activation under visible light irradiation [5,6]. Enabling the use of the natural sunlight irradiation would reduce operational expenditure, providing the opportunity for technology adaptation by regions with high solar radiation

according to solar maps. For example, the northeastern region of Brazil receives >22 MJ m^2 of sunlight irradiation annually due to its proximity to the equatorial line, which corresponds to approximately 10 h of sunlight every day [7].

Niobium-based oxide semiconductors have promising characteristics for environmental applications due to their hypoallergenic character, low cytotoxicity, and physiological and chemical inertness, along with their high thermodynamic stability [8,9]. However, the most remarkable aspect for their application in Brazil is their wide availability in the country, which is the major producer of niobium worldwide, with 99.0% of the world's niobium being located in Brazil [10]. Sustainable exploitation of this resource for environmental applications may positively affect socio-economic aspects, since few applications of niobium have been identified.

Brazil is the fourth biggest cotton textile exporter worldwide and the fifth biggest global manufacturer. Textile fiber dyeing process requires large volumes of water, resulting in the release of large amounts of colored wastewater effluent [11,12]. Green and sustainable manufacturing approaches require the minimization of the usage of water resources. Removal of organic dyes can incentivize water reuse in dyeing baths [13]. Photocatalytic treatment could be a suitable low-cost alternative for small/mid-sized Brazilian textile facilities [14,15]. Photocatalytic treatment is classified as an Advanced Oxidation Process, since it allows the in situ generation of highly oxidant species such as hydroxyl radicals ($^{\bullet}OH$) [16,17]. The light irradiation of a semiconductor with photons with a higher energy than its band gap enables the photo-excitation of an electron from the filled valence band of the semiconductor to the empty conduction band (e_{cb}^-), leaving a positively charged vacancy or hole (h_{vb}^+) following Reaction (1) [18,19]. Organic pollutants (i.e., dyes) can then be oxidized by the photogenerated hole, as well as by heterogeneous $^{\bullet}OH$ formed on the photocatalyst surface from the water oxidation by the h_{vb}^+ according to Reaction (2) [20,21].

$$\text{Semiconductor} + h\nu \rightarrow h_{vb}^+ + e_{cb}^- \quad (1)$$

$$h_{vb}^+ + H_2O \rightarrow {}^{\bullet}OH + H^+ \quad (2)$$

The recombination of e_{cb}^- with unreacted h_{vb}^+ through Reaction (3) is responsible for the oxidative power loss in photocatalytic systems [22,23]. Dissolved oxygen can react with e_{cb}^-, yielding superoxide radicals ($O_2^{\bullet-}$) through Reaction (4), which contributes to slowing down the recombination reaction [24,25]. However, the use of e_{cb}^- scavengers can further minimize the extent of this undesirable reaction while enhancing performance. For example, the weak oxidant H_2O_2 can react with e_{cb}^- and $O_2^{\bullet-}$, producing additional $^{\bullet}OH$ from Reactions (5) and (6), respectively [26].

$$e_{cb}^- + h_{vb}^+ \rightarrow \text{heat} \quad (3)$$

$$e_{cb}^- + O_2 \rightarrow O_2^{\bullet-} \quad (4)$$

$$e_{cb}^- + H_2O_2 \rightarrow {}^{\bullet}OH + OH^- \quad (5)$$

$$O_2^{\bullet-} + H_2O_2 \rightarrow {}^{\bullet}OH + OH^- + O_2 \quad (6)$$

Dye bath effluent decolorization enables water reuse for additional textile dyeing processes, minimizing the environmental footprint and the capital costs associated with water usage. This work studies the applicability of novel niobium oxide photocatalysts (Nb_2O_5) in the efficient decolorization of wastewaters containing azo-dyes. The synthesized materials were characterized in accordance with calcination methodologies. Decolorization capabilities were evaluated, and operational variables were optimized. This innovative alternative for water treatment processes, which is emerging as a new trend in photocatalytic technologies, meets sustainable technology manufacturing needs through the use of regionally abundant natural resources.

2. Results and Discussions

2.1. Characterization of Nb_2O_5 Photocatalyst

The synthesized Nb_2O_5 photocatalyst powder was characterized by SEM. The micrograph in Figure 1a exhibits a uniform particle size distribution of ca. 200 nm. The magnified catalyst surface depicted in Figure 1b exhibits a high roughness and porosity, which could be induced by the calcination process of the niobium oxalate complex ammonium salt. The mapping of the chemical composition of the catalyst particles (Figure 1c) indicated that they are composed of niobium with a homogenous distribution.

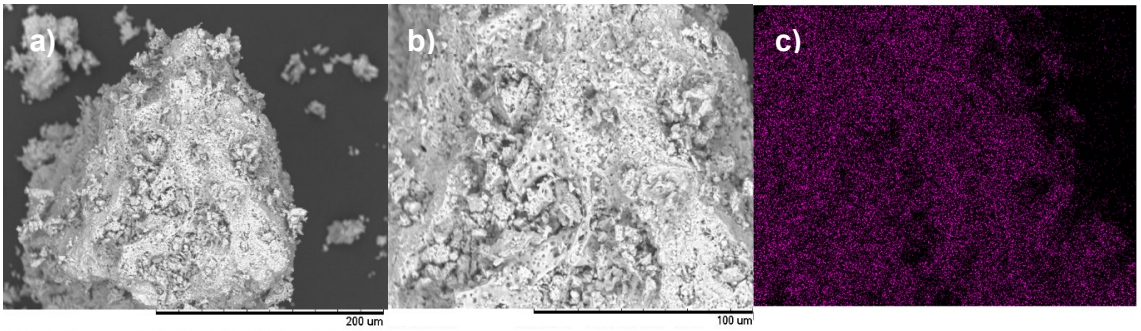

Figure 1. Scanning electron micrographs of Nb_2O_5-synthesized photocatalyst with magnifications of (**a**) 500× and (**b**) 1000×, and (**c**) niobium mapping micrograph.

The FTIR spectrum of Nb_2O_5 in Figure 2 depicts the characteristic bands of niobium oxides: one shoulder at 900 cm^{-1} is attributed to the stretch Nb-O and the bands at 661 and 600 cm^{-1} are attributed to the angular vibration Nb-O-Nb [27]. Additionally, a band can be observed at 1622 cm^{-1} that is related to the water adsorbed on the surface of Nb_2O_5 [8,28], and a small band can be observed at 1531 cm^{-1} that is usually associated with impurities from the precursor salt of niobium. These impurities in the precursor are considered to be beneficial in the literature, since they act as stabilizers of the niobium oxide catalyst [29,30].

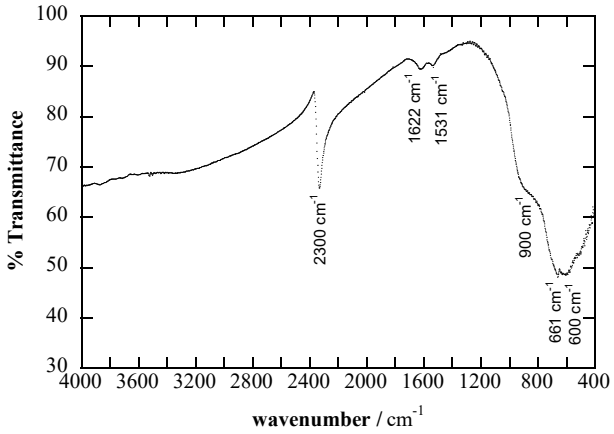

Figure 2. FTIR spectra of synthesized Nb_2O_5.

Niobium oxide has a complex crystal morphology, wherein at least 12 crystallographic structures have been identified to date [31]. The X-ray diffraction pattern obtained from the synthesized Nb_2O_5 powder catalyst is shown in Figure 3a. It can be seen that the diffractogram presents reflections 2θ = 22.6°, 28.5°, 36.7°, 46.3°, 50.4°, and 55.3°, which correspond to the crystallographic planes of miller index (001), (100), (101), (002), (110), and (102), respectively. These planes are characteristic of the pseudohexagonal structure of niobium oxide [27,32], proving the obtention of a catalyst with

a defined crystalline microstructure with a crystallite size of 2.2 nm estimated from the Scherrer formula. The electronic spectroscopy of diffuse reflectance made it possible to determine the band-gap energy required for the photo-promotion of one electron (see Figure 3b). The results indicated that Nb_2O_5 presents a band gap of 3.1 eV, similar to the characteristic band gap of titanium dioxide photocatalysts [9,33], and at the low end of the Nb_2O_5 bandgap values [34].

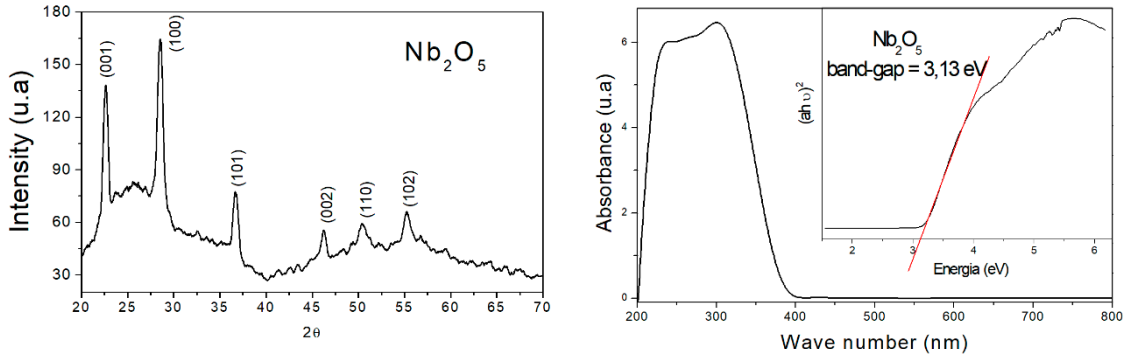

(**a**) (**b**)

Figure 3. (**a**) X-ray diffractogram of Nb_2O_5. (**b**) UV-vis DRS absorption spectra of synthesized Nb_2O_5. The inset panel shows the Tauc plot for the band-gap energy determination of 3.13 eV.

The isotherm of nitrogen adsorption-desorption of Nb_2O_5 in Figure 4a presents a hysteresis loop characteristic of type IV isotherms, which is typical of mesoporous materials. This is in agreement with the characteristic morphologies observed by SEM in Figure 1. The specific surface area of 42.36 m^2 g^{-1} was calculated from the BET method (S_{BET}). Meanwhile, the BJH analysis (Figure 4b) revealed the presence of uniformly sized mesopores with an average diameter (d_p) of 10.1 nm and a mean pore volume (V_p) equal to 0.102 cm^3 g^{-1}. These results are in agreement with those reported by Wang et al. [32] for commercial niobium oxide calcined at a temperature of 500 °C (S_{BET} = 49.9 m^2 g^{-1}, V_p = 0.12 cm^3 g^{-1} e d_p = 9.6 nm), even when the niobium oxide precursor selected was different.

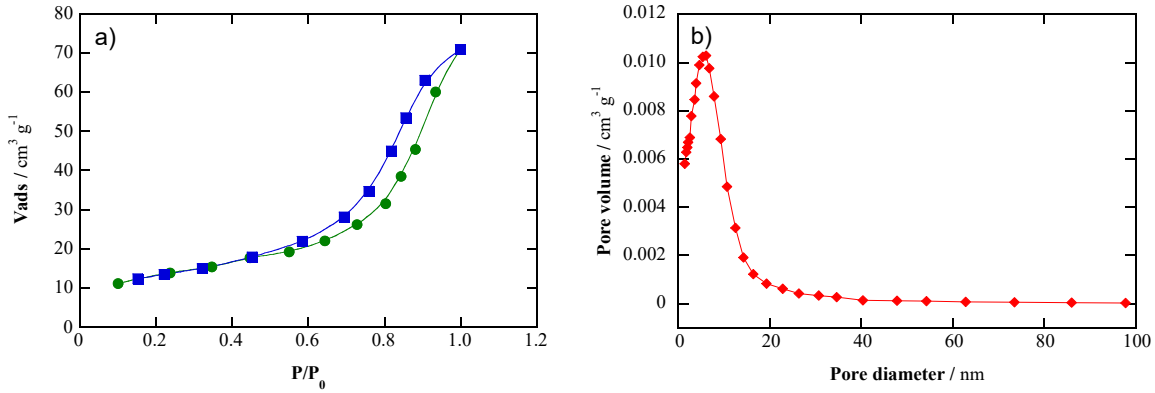

(**a**) (**b**)

Figure 4. (**a**) Nb_2O_5 photocatalyst nitrogen (●) adsorption–(■) desorption isotherms. (**b**) Pore size distribution plot that depicts the characteristic response of mesoporous materials.

2.2. Photocatalytic Activity on Azo Dye Decolorization

The photocatalytic activity of the synthesized Nb_2O_5 was verified on the basis of the corresponding decolorization of solutions containing 5 mg L^{-1} methyl orange (MO) as model azo dye (see Table 1). MO is highly photostable, and is not degraded under direct sunlight irradiation, as depicted in Figure 5 [12]. Meanwhile, ca. 6.0% decolorization after 100 min was observed when 1.0 g L^{-1} of Nb_2O_5 catalyst suspended in solution was exposed to sunlight irradiation. Photocatalytic degradation

can be assumed, since only a discrete 0.6% removal was observed under dark conditions due to adsorption on the porous Nb_2O_5. The slight photocatalytic removal under solar irradiation could be justified by the faster recombination Reaction (3), which diminishes the available oxidants (i.e., h_{vb}^+ and $^{\bullet}OH$) [17,22]. The strategic use of selective e_{cb}^- scavengers may synergistically enhance the photocatalytic response by inhibiting the extent of Reaction (3) [16,26]. As shown in Figure 5, the addition of H_2O_2 boosts the performance of Nb_2O_5, which attains complete decolorization after 40 min. It is important to remark that the sole addition of H_2O_2 under dark conditions had no effect on dye solution decolorization, because of the weak oxidative capacity of H_2O_2 ($E^o(H_2O_2/H_2O)$ = 1.76 V/SHE). Nevertheless, decolorization was observed in the presence of H_2O_2 under direct solar irradiation due to the photolytic decomposition of H_2O_2 according to Reaction (7). Please note that this reaction only occurs under UVC irradiation, which is a component of the solar light in Northeast Brazil [24,35].

$$H_2O_2 + h\nu \rightarrow 2\,^{\bullet}OH \quad (7)$$

Table 1. Chemical structure and characteristics of Methyl Orange azo dye.

Property	Characteristics
IUPAC name	Sodium 4-{[4-(dimethylamino) phenyl] diazenyl} benzene-1-sulfonate
Common name	Methyl Orange
CAS number	547-58-0
Color Index number	13,025
M/g mol^{-1}	327.3
λ_{max}/nm	464
pK_a	3.45
Chemical formula	$C_{14}H_{14}N_3SO_3Na$
Chemical structure	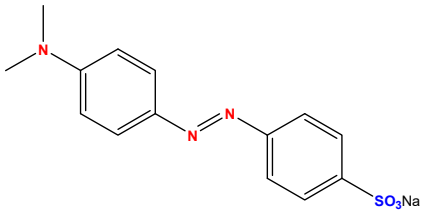

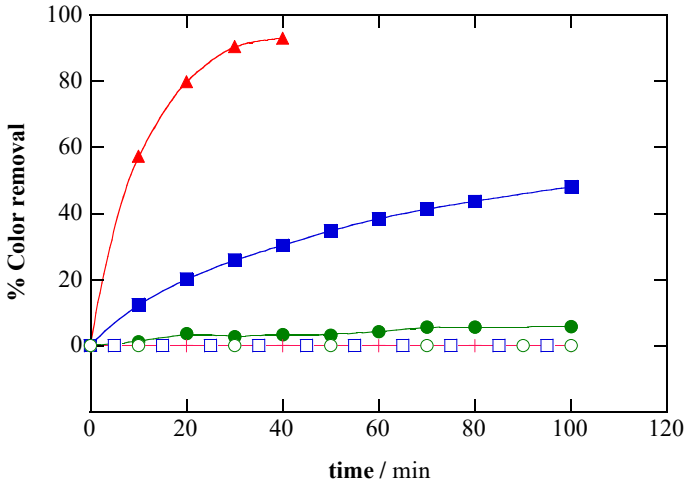

Figure 5. Evaluation of the photocatalytic degradation of 100 mL of 5 mg L^{-1} of MO at pH 5.0 with (○, ●) 1.0 g L^{-1} of Nb_2O_5, (□, ■) 0.20 M H_2O_2, (△, ▲) Nb_2O_5 g L^{-1} with 0.20 M H_2O_2, (○, □, △) in dark conditions or (●, ■, ▲) under sunlight irradiation. The photostability of the dye solution was also tested (**+**).

The synergetic effect observed between Nb_2O_5 and e_{cb}^- scavenger H_2O_2 can be explained by the enhanced generation of $^{\bullet}OH$ from Reaction (2) due to the significant reduction of the recombination rate of Reaction (3) [26,36]. This effect results in a consequent increase in the availability of reactive oxygen species on the Nb_2O_5 photocatalyst surface, and then the increased oxidation capabilities of the system degrading the azo dye molecule [17,23].

The synergetic effect of H_2O_2 evidences its role in Nb_2O_5 photocatalytic efficiency performance. For this reason, the role of H_2O_2 concentration in solution was studied as a rate driving parameter for decolorization. Figure 6 shows the percentage of color removal attained for increasing doses of H_2O_2 acting as e_{cb}^- scavenger. Higher color removal percentages of 6.0%, 71.5% and 91.0% were observed for increasing concentrations of H_2O_2 of 0 M, 0.10 M and 0.20 M, respectively. It should be noted that further increase in H_2O_2 concentration resulted in a decrease in performance, achieving a lower color removal of only 77.2% after 80 min of Nb_2O_5 photocatalytic treatment. This phenomenon can be explained by the acceleration of concomitant waste reactions [17,37]. One of the main processes that decreases performance is the oxidation of excess H_2O_2 by $^{\bullet}OH$ following Reaction (8) [24,26]. This undesired side-reaction not only consumes $^{\bullet}OH$, which will subsequently not be able to oxidize the target azo dye, but it also diminishes the available amount of H_2O_2. Moreover, the excessive accumulation of radical species can promote their dimerization following Reactions (9) and (10) [12,38]. These undesired reactions do not contribute to the overall photocatalytic performance, and may slow down the decolorization kinetics, as was observed experimentally (see Figure 6). Therefore, an optimal dose of 0.2 M H_2O_2 was defined for the following experiments to ensure faster solution decolorization and higher photocatalytic efficiency.

$$H_2O_2 + {}^{\bullet}OH \rightarrow HO_2^{\bullet} + H_2O \quad (8)$$

$$HO_2^{\bullet} + {}^{\bullet}OH \rightarrow H_2O + O_2 \quad (9)$$

$$2\,{}^{\bullet}OH \rightarrow H_2O_2 \quad (10)$$

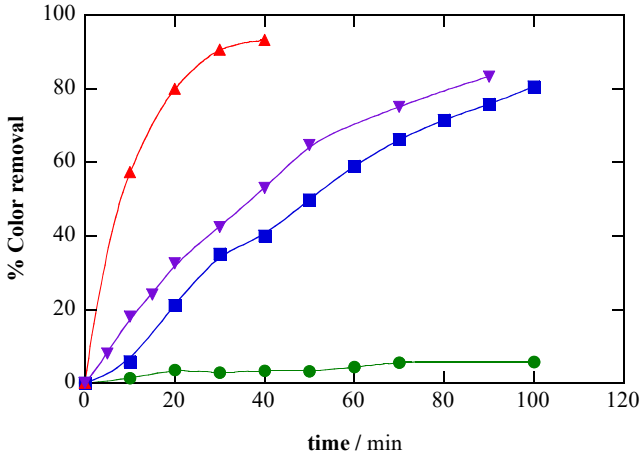

Figure 6. Impact of the e_{cb}^- scavenger dose on the solar photocatalytic decolorization of 100 mL of 5 mg L^{-1} of MO with 1.0 g L^{-1} of Nb_2O_5 at pH 5.0. Initial H_2O_2 concentration: (●) 0 M, (■) 0.10 M, (▲) 0.20 M, and (▼) 0.30 M.

2.3. Effect of pH on the Photocatalytic Decolorization of Azo Dye Methyl Orange

The pH of the treated solution is one of the variables with the greatest influence on the photocatalytic degradation of pollutants, because it affects several physical-chemical properties of the catalysts that enhance or reduce the degradation efficiency, including the catalyst surface charge and the organic adsorptivity [17,23,39]. The point of zero charge (PZC) pH_{PZC} = 4.86 of Nb_2O_5 was determined by the pH drift method [24,40], as described in the methodology section. The pH_{PZC} is an intrinsic

characteristic of the catalyst that makes it possible to determine whether the surface of Nb_2O_5 is negatively or positively charged as a function of the pH. If the working pH conditions are above of the pH_{PZC} of the Nb_2O_5, the catalyst surface is negatively charged. Conversely, the surface will be positively charged when the pH is below the pH_{PZC}.

Figure 7 shows the effect of the initial pH on the decolorization efficiency of MO using 1.0 g L^{-1} of Nb_2O_5 photocatalyst and 0.20 M of H_2O_2. It is important to note that in the range of pH under consideration, the sulfonic group of azo dye MO is deprotonated, with the pollutant molecule being negatively charged (see Table 1). However, at pH = 3.0, one of the molecule's N is protonated, and the global charge of the molecule will be neutral (pK_a = 3.45). This consideration is an important fact that could justify the lower decolorization achieved at alkaline pH. Above the pH_{PZC}, the Nb_2O_5 surface is negatively charged, and the dye molecule will also be negatively charged, thus leading to electrostatic charge repulsion, making the adsorption processes more difficult, along with the approach of the molecule towards the photocatalyst surface. Thus, with increasing values of pH, the number of negatively charged sites on the Nb_2O_5 also increases, further reducing the photodecolorization process in the following sequence 7.0 > 9.0 > 11.0, with percentages of color removal of 39.3%, 16.0% and 7.5%, respectively. In addition, it is well known that the rate of decomposition of unstable H_2O_2 increases with increasing pH in accordance with Equations (11) or (12) in strongly alkaline media [41]. This loss of H_2O_2 by chemical decomposition affects the overall photocatalytic performance. First, it reduces the availability of e_{cb}^- scavenger in solution. Second, it consequently reduces the generation of $^{\bullet}OH$ radicals. In contrast, at pH 3.0, the surface is positively charged. This stimulates the molecules' approach to and absorption onto the surface through the negatively charged sulfonic group. Thus, below pH 3.0, complete color removal can be achieved at lower treatment times of 10 min.

$$2\,H_2O_2 \rightarrow 2\,H_2O + O_2 \tag{11}$$

$$HO_2^- \rightarrow OH^- + \frac{1}{2}\,O_2 \tag{12}$$

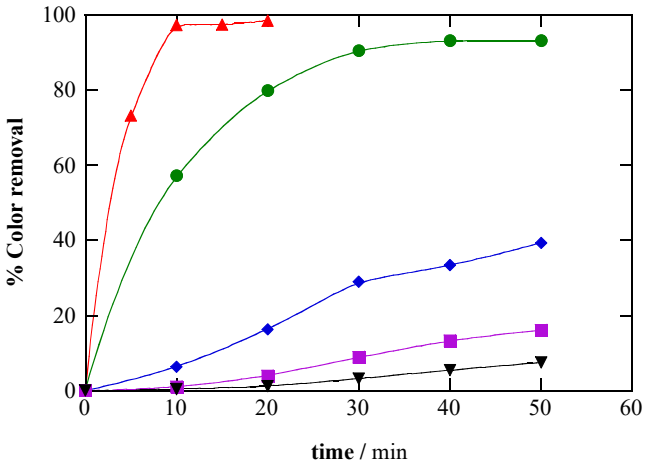

Figure 7. Influence of the initial pH on the percentage of color removal during solar photocatalytic treatment of 100 mL of 5 mg L^{-1} of MO with 1.0 g L^{-1} of Nb_2O_5 0.2 M of H_2O_2 at pH: (▲) 3.0, (●) 5.0, (♦) 7.0, (■) 9.0 and (▼) 11.0.

The nearest working pH to pH_{PZC} = 4.86 was 5.0. Under these conditions, the catalyst surface is practically neutral and has no electro-attractive or electro-repulsive effects that affect the adsorption processes. Thus, as observed in Figure 7, it presents faster decolorization kinetics than higher, more alkaline pH, but slightly slower kinetics than those obtained for pH 3.0. The pH 5.0 was considered the optimum condition, because it is the natural pH of MO solutions and the nearest to the circumneutral pH of water effluents. This would decrease the potential environmental health and safety risks, as well

as the costs to small/mid-sized industry, by minimizing the handling and storage of acids and bases. Furthermore, this may have an impact on operational costs, since it would obviate acidification for the treatment and neutralization steps prior to the release of treated effluent.

2.4. Evaluation of Optimal Dosage of Nb_2O_5 to Ensure Maximum Performance

Optimizing the dosage of catalysts is a critical engineering parameter when designing sustainable reactors for solar photocatalytic applications at large scale [16,17]. The impact of Nb_2O_5 dose on decolorization kinetics was evaluated within the range from 0.25 g L^{-1} up to 2.00 g L^{-1} by treating solutions of 5 mg L^{-1} of MO azo dye at pH 5.0 in the presence of 0.20 M of H_2O_2. Figure 8 reports an enhancement in the decolorization rate with increasing dosage of Nb_2O_5. These improved performances can be explained due to the increasing number of active sites resulting from the higher total specific surface of Nb_2O_5 available, thereby accelerating the photocatalytic generation of oxidants in solution by Reactions (1) and (2). The effective reduction of photocatalytic efficiency at excessively high catalyst dosages is commonly reported in the literature, and is attributed to the detrimental effects on light transport in solution caused by: (i) the increase of the solution opacity, which diminishes the radiation penetration and consequently the photogeneration of vacancies [9,40]; (ii) the aggregation of suspended catalyst particles diminishing the specific area [27,36]; and (iii) light scattering effects that also reduce the UV light penetration [22,42]. In addition, the surface available for adsorption processes is also increased, favoring the mechanisms of organic degradation. However, in our experiments, no appreciable loss of efficiency was observed, although the decolorization rate increase became lower from 1 g L^{-1}, resulting in a plateau. The kinetic analysis of MO color removal enabled the estimation of pseudo-first-order rate constants of decolorization (k_{dec}). These analyses showed excellent fits for a pseudo-first-order reaction, assuming that the $^{\bullet}OH$ radicals achieve a pseudo-constant concentration on the Nb_2O_5 surface. Increasing k_{dec} of $3.18 \cdot 10^{-4}$ s^{-1} ($R^2 = 0.996$) with 0.25 g L^{-1} of Nb_2O_5, $6.12 \cdot 10^{-4}$ s^{-1} ($R^2 = 0.997$) with 0.50 g L^{-1} of Nb_2O_5, $1.00 \cdot 10^{-3}$ s^{-1} ($R^2 = 0.997$) with 1.00 g L^{-1} of Nb_2O_5 and $1.07 \cdot 10^{-3}$ s^{-1} ($R^2 = 0.998$) with 0.25 g L^{-1} of Nb_2O_5 were observed. It is important to remark that the slight increase in decolorization rate from 1.0 to 2.0 g L^{-1} is presumably related to the loss of photocatalytic efficiency at excessively high catalyst dosages. Thus, a catalyst dosage of 1.0 g L^{-1} was identified as the optimal condition, because it is the lowest dosage at which a faster decolorization rate can be achieved.

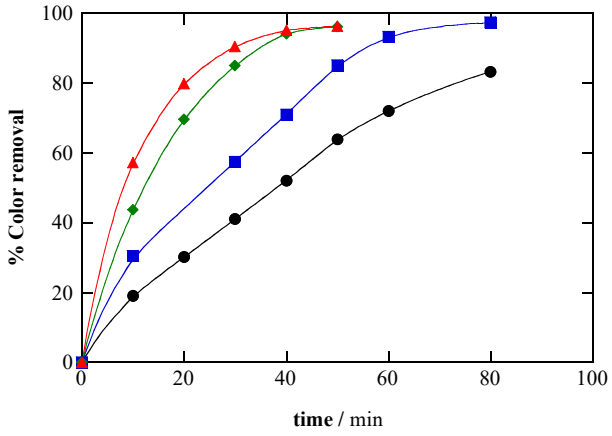

Figure 8. Influence of Nb_2O_5 photocatalyst dose on the photocatalytic performance. Dosing: (●) 0.25 g L^{-1}, (■) 0.5 g L^{-1}, (♦) 1.0 g L^{-1}, and (▲) 2.0 g L^{-1}.

2.5. Effect of Initial Dye Concentration on Nb_2O_5 Performance

The initial dye concentration is a variable of interest that gives invaluable information about the range of pollutant concentration that is efficiently treatable within a reasonable timeframe. For this reason, MO solutions of 5, 10, 15 and 30 mg L^{-1} were treated under the optimum conditions of pH 5.0 with 0.20 M of H_2O_2 and 1.0 g L^{-1} of Nb_2O_5 photocatalyst. Figure 9 depicts the abatement of

dye concentration as a function of photocatalytic treatment time for different initial concentrations of MO. The estimation of k_{dec} exhibits variation over an order of magnitude when increasing the dye concentration. Decreasing k_{dec} values from $1.07 \cdot 10^{-3}$ s^{-1} ($R^2 = 0.998$) for 5.0 mg L^{-1} of MO, $4.37 \cdot 10^{4}$ s^{-1} ($R^2 = 0.999$) for 10.0 mg L^{-1} of MO, $2.17 \cdot 10^{-4}$ s^{-1} ($R^2 = 0.996$) for 15.0 mg L^{-1} of MO, down to $1.01 \cdot 10^{-4}$ s^{-1} ($R^2 = 0.993$) for 30.0 mg L^{-1} of MO were estimated as depicted in the inset panel of Figure 9. The greater azo dye concentration implies a greater colorization of the water being treated, thus limiting the light penetration into the solution and diminishing photocatalytic Reactions (1) and (2), which generate oxidant species. Furthermore, the greater accumulation of organic intermediates susceptible adsorption onto the Nb_2O_5 active sites could inhibit the photocatalytic generation of vacancies and the production of other oxidants, decreasing the organic events and, consequently, the decolorization rate [9,23,43]. Therefore, longer treatment times would be required to completely decolorize MO at higher pollutant loads.

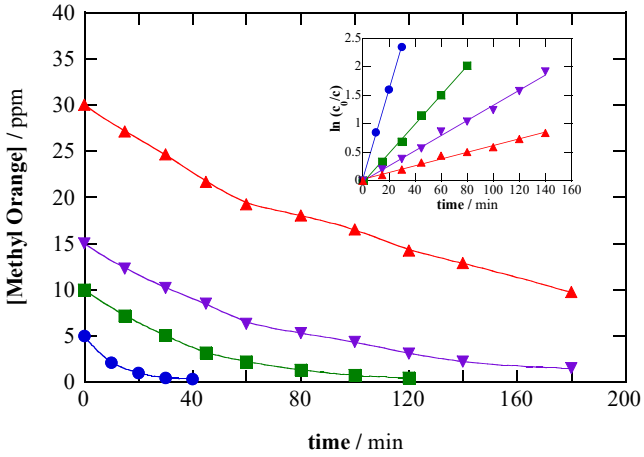

Figure 9. Methyl Orange azo dye abatement vs photoelectrocatalytic treatment time of 100 mL of solution with 1.0 g L^{-1} of Nb_2O_5, 0.20 M of H_2O_2 at pH 5.0 and dye concentration of: (●) 5 mg L^{-1}, (■) 10 mg L^{-1}, (▼) 15 mg L^{-1} and (▲) 30 mg L^{-1}. The corresponding kinetic analysis assuming a pseudo-first-order reaction for MO is given in the inset panel.

2.6. Evaluating Reutilization Capabilities of Nb_2O_5 Catalyst Aiming for Sustainable Implementation and Comparison with Other Catalysts' Performance

Sustainable processes must consider the continuous reutilization of photocatalytic materials within catalytic converters [44]. Reutilization capabilities and stabilities of novel materials should be assessed in order to demonstrate material stability. Therefore, Nb_2O_5 was submitted to continuous treatment operation. Suspended Nb_2O_5 photocatalyst was recovered and tested over consecutive decolorization cycles of MO solutions. As depicted in Figure 10, the niobium metal oxide semiconductor presented excellent stability, and retained its catalytic properties over 10 cycles. Please note that consecutive cycles demonstrated reproducible MO removal performance. It is important to remark that previous reports in the literature reported higher stability of niobium oxides than for conventional TiO_2 or ZnO catalysts [9,27,28]. In this context, the results reported here support these previous studies, indicating Nb_2O_5 as an emerging photocatalyst for environmental remediation. However, more studies related to catalyst aging and fouling during continuous operation are required to ensure the lifetime of these emerging catalysts.

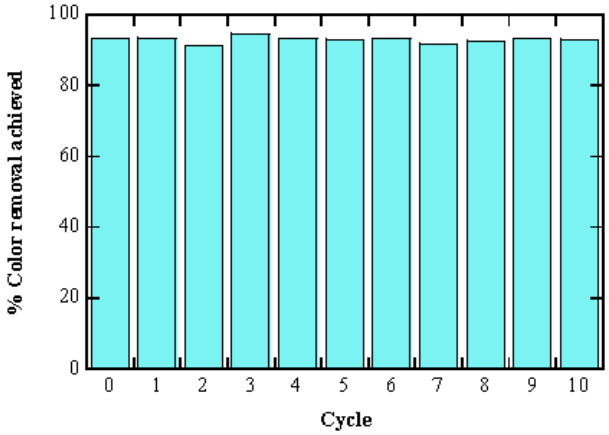

Figure 10. Percentage of color removal achieved after 40 min of solar photoelectrocatalytic treatment of 5 mg L^{-1} of MO with 1.0 g L^{-1} of catalyst Nb_2O_5 in slurry at pH 5.0 with 0.20 M of H_2O_2 after consecutive reuse of Nb_2O_5.

A quick comparison with other photocatalytic materials reported in the literature demonstrates the promising performance of novel niobium oxide semiconductors for water treatment applications. As summarized in Table 2, the results reported in this work are highly competitive, since Nb_2O_5 makes it possible to reduce operational times by more than half when compared with doped TiO_2 and other complex mixed oxides.

Table 2. Comparative performance of visible photocatalytic decolorization of Methyl Orange azo dye with different catalysts to attain over 95% color removal.

Photocatalysts	[Methyl Orange]/mg L^{-1}	Decolorization Time/Min	References
Pd-doped TiO_2	20	150	[45]
Cu-doped TiO_2	10	140	[46]
Cu-doped ZnO	13	120	[47]
Ag/TiO_2	20	120	[48]
Bi_3TiNbO_9	10	75	[49]
Nb_2O_5	10	65	This work

3. Materials and Methods

3.1. Chemicals

MO azo dye of 85.0% purity and the H_2O_2 of 33% (*w*/*w*) were supplied by Sigma-Aldrich. The ammonium salt of the niobium oxalate complex ($NH_4[NbO(C_2O_4)_2(H_2O)]$. $3H_2O$) of 99.0% purity used in the photocatalyst synthesis was purchased from CBMM. The pH was adjusted prior to experiments using H_2SO_4 or NaOH of analytical grade, supplied by Sigma-Aldrich. All solutions were prepared with high-purity water obtained from a Millipore Milli-Q system with resistivity >18 MΩ cm at 25 °C.

3.2. Synthesis of Microparticulated Nb_2O_5 Photocatalyst

The ammonium salt of the niobium oxalate complex was calcined using a temperature ramp of 10 °C min^{-1} to 500 °C, where it remained for 4 h under ambient atmosphere. Under these conditions, the oxalate was completely incinerated, leading to the formation of amorphous Nb_2O_5 photocatalyst.

3.3. Solar Photocatalytic Experiences

The photochemical reactor used during photocatalytic experiments consisted of an undivided open cell directly exposed to sunlight. The photocatalyst was suspended in the solution in slurry

and the tests were carried out under vigorous stirring with a magnetic bar at 700 rpm to ensure the homogeneous distribution of the catalyst in the bulk, while also favoring the transport of reactants to/from the catalyst surface. The photochemical cell had a double jacket in which water was circulated to maintain the solution temperature at 25 °C using a LAUDA A100 thermostat, avoiding the evaporation of the treated solution by solar irradiation heating. Prior to the photocatalytic experiments, the solutions were maintained at the defined pH, dye and catalyst concentration conditions for 30 min in the dark.

3.4. Apparatus and Analytical Procedures

Scanning electron microscopy (SEM) micrographies of the synthesized Nb_2O_5 photocatalyst were obtained using a Hitachi TM-3000 system with a frequency of 50/60 Hz and a magnification capacity of up to 3000x. The X-ray diffractogram (XRD) patterns were recorded on a Bruker D2 Phaser diffractometer with Cu-K_α (λ = 1.54 Å) irradiation source using a Ni filter and a Lynxeye detector, performing the analysis in the 2θ range from 2° to 70°. The average crystallite sizes were estimated by applying Scherrer's Formula (13) to the identified crystal planes [50,51]:

$$\tau = K\,\lambda/\beta\,\cos\theta \quad (13)$$

where τ refers to the mean size of the ordered crystalline domains, K is the Scherrer constant, a dimensionless shape factor that usually has values close to unity, λ is the X-ray wavelength, β is the line width at half maximum in radians and θ is the Bragg angle in degrees.

Fourier transform infrared (FTIR) spectra were recorded from a Shimadzu-8400S FTIR spectrometer in the medium IR region (4000–400 cm^{-1}) after 30 scans with a resolution of 4 cm^{-1}. The UV-vis diffuse reflectance spectra between 200–600 nm, used to determine the band gap from solid samples on the basis of Kubelka-Munk and Tauc plots [52], was obtained with a UV-vis spectrometer Cary 500 Scan using the barium sulfate pattern as a reference material. The specific surface area was determined on the basis of nitrogen adsorption-desorption isotherms registered on a Micrometrics ASAP 2020. The Nb_2O_5 catalyst samples were previously degassed at 300 °C for 3 h and subsequently submitted to a nitrogen atmosphere at 77 K. The nitrogen adsorption-desorption curve made it possible to determine the specific surface by area using BET method in the region of low relative pressure (p/p_0 = 0.1–1.0). The Barret–Joyner–Halenda method (BJH) was used to determine the pore size distribution.

The pH of the treated solutions was adjusted using a pH-meter Tecnopon mPA-210. The percentage of color removal for the solution during the photocatalytic treatment was estimated using Equation (14) [12,53]:

$$\%\text{Color Removal} = (A_0 - A_t)/A_0 \times 100 \quad (14)$$

where A_0 is the initial absorbance and A_t the absorbance at the treatment time *t*. The absorbance was determined at the maximum absorptivity of MO (λ_{max} = 642 nm) using a UV-vis spectrophotometer Analytikjena SPECORD 210 PLUS. The point of zero charge (PZC) of Nb_2O_5 was determined by the pH drift method, as described by Hashemzadeh et al. [40]. Solutions of 50 mL of 0.01 M of NaCl where adjusted to different pH between 1 and 11 by adding HCl or NaOH. After achieving the defined initial pH, 0.05 g of Nb_2O_5 photocatalyst was added to the solution, which was maintained at 25 °C for 48 h under constant stirring at 700 rpm before measuring the solution pH to determine the pH_{final}. The pH_{PZC} was determined from the intersection of the curve pH_{final} vs. $pH_{initial}$ with the straight line $pH_{final} = pH_{initial}$.

4. Conclusions

The potential application of Nb_2O_5 for photocatalytic decontamination and decolorization of wastewater containing azo dyes was proved on basis of the efficient removal of a model pollutant: MO. A novel Nb_2O_5 photocatalyst was successfully synthesized using a facile calcination method from a natural precursor extracted as a natural resource in Brazil and characterized. The photocatalytic assays demonstrated high removal efficiency of MO azo dye in the presence of H_2O_2, which was used as

an e_{cb}^- scavenger, and oxidants, which acted as a photogeneration enhancer. The effects of different control parameters were analyzed and optimized to enable the faster decolorization under the mildest conditions. Thereby, a concentration of Nb_2O_5 catalyst of 1.0 g L^{-1} in slurry was identified as the optimal conditions for the complete removal of color at lower catalyst dosages. The tests carried out also defined as optimal the mild conditions of pH 5.0 and 0.20 M of H_2O_2, with treatable concentrations of MO ranging up to 15 mg L^{-1}. It should be noted that the study was developed in order to find potential applications for niobium materials, which represent a key material produced extensively in Brazil. Our results prove the promising applicability of these innocuous and highly re-utilizable photocatalysts in AOPs for wastewater treatment. It is worth mentioning that this technique is emerging as suitable approach for depollution treatment of textile effluent in mid-sized industry in the Northeast region of Brazil, which receives approximately 10 h/day of sunlight irradiation for more than 350 days a year due to its proximity to the equatorial line.

Author Contributions: Conceptualization: A.J.d.S. and S.G.-S.; methodology: A.J.d.S., L.M.B.B. and S.G.-S.; validation: A.J.d.S., C.A.M.-H. and A.P.d.M.A.; formal analysis: A.J.d.S., S.G.-S. and C.A.M.-H.; investigation: A.J.d.S., L.M.B.B. and S.G.-S.; resources: C.A.M.-H. and A.P.d.M.A.; data curation: A.J.d.S., L.M.B.B. and S.G.-S.; writing—original draft preparation: A.J.d.S. and S.G.-S.; writing—review and editing: C.A.M.-H., A.P.d.M.A. and S.G.-S.; visualization; A.J.d.S. and L.M.B.B.; supervision: C.A.M.-H., A.P.d.M.A. and S.G.-S.; project administration: C.A.M.-H. and A.P.d.M.A.; funding acquisition: C.A.M.-H., A.P.d.M.A. and S.G.-S.

Funding: Financial supports from National Council for Scientific and Technological Development (CNPq—465571/2014-0; CNPq—446846/2014-7 and CNPq—401519/2014-7) and FAPESP (2014/50945-4) are gratefully acknowledged. A.J. dos Santos and L.M.B. Batista gratefully acknowledge the grants awarded from CAPES.

Conflicts of Interest: The authors declare no conflict of interest.

References

1. Nakata, K.; Fujishima, A. TiO_2 photocatalysis: Design and applications. *J. Photochem. Photobiol. C Photochem. Rev.* **2012**, *13*, 169–189. [CrossRef]
2. Garcia-Segura, S.; Brillas, E. Applied photoelectrocatalysis on the degradation of organic pollutants in wastewaters. *J. Photochem. Photobiol. C Photochem. Rev.* **2017**, *31*, 1–35. [CrossRef]
3. Kirner, J.T.; Finke, R.G. Water-oxidation photoanodes using organic light-harvesting materials: A review. *J. Mater. Chem. A* **2017**, *5*, 19560–19592. [CrossRef]
4. Kawamura, G.; Matsuda, A. Synthesis of plasmonic photocatalysts for water splitting. *Catalysts* **2019**, *9*, 982. [CrossRef]
5. Cerrón-Calle, G.A.; Aranda-Aguirre, A.J.; Luyo, C.; Garcia-Segura, S.; Alarcón, H. Photoelectrocatalytic decolorization of azo dyes with nano-composite oxide layers of ZnO nanorods decorated with Ag nanoparticles. *Chemosphere* **2019**, *219*, 296–304. [CrossRef]
6. Loeb, S.K.; Alvarez, P.J.J.; Brame, J.A.; Cates, E.L.; Choi, W.; Crittenden, J.; Dionysiou, D.D.; Li, Q.; Li-puma, G.; Quan, X.; et al. The Technology Horizon for Photocatalytic Water Treatment: Sunrise or Sunset? *Environ. Sci. Technol.* **2019**, *53*, 2937–2947. [CrossRef]
7. Simioni, T.; Schaeffer, R. Georeferenced operating-efficiency solar potential maps with local weather conditions—An application to Brazil. *Sol. Energy* **2019**, *184*, 345–355. [CrossRef]
8. Prado, N.T.; Oliveira, L.C.A. Nanostructured niobium oxide synthetized by a new route using hydrothermal treatment: High efficiency in oxidation reactions. *Appl. Catal. B Environ.* **2017**, *205*, 481–488. [CrossRef]
9. Hashemzadeh, F.; Gaffarinejad, A.; Rahimi, R. Porous p-NiO/n-Nb_2O_5 nanocomposites prepared by an EISA route with enhanced photocatalytic activity in simultaneous Cr(VI) reduction and methyl orange decolorization under visible light irradiation. *J. Hazard. Mater.* **2015**, *286*, 64–74. [CrossRef]
10. Gibson, C.E.; Kelebek, S.; Aghamirian, M. Niobium oxide mineral flotation: A review of relevant literature and the current state of industrial operations. *Int. J. Miner. Process.* **2015**, *137*, 82–97. [CrossRef]
11. Garcia, S.; Cordeiro, A.; de Nääs, I.A.; de Neto, P.L.O.C. The sustainability awareness of Brazilian consumers of cotton clothing. *J. Clean. Prod.* **2019**, *215*, 1490–1502. [CrossRef]
12. Brillas, E.; Martínez-Huitle, C.A. Decontamination of wastewaters containing synthetic organic dyes by electrochemical methods. An updated review. *Appl. Catal. B Environ.* **2015**, *166*, 603–643. [CrossRef]

13. Mansour, F.; Alnouri, S.Y.; Al-Hindi, M.; Azizi, F.; Linke, P. Screening and cost assessment strategies for end-of-Pipe Zero Liquid Discharge systems. *J. Clean. Prod.* **2018**, *179*, 460–477. [CrossRef]
14. Soares, P.A.; Silva, T.F.C.V.; Ramos Arcy, A.; Souza, S.M.A.G.U.; Boaventura, R.A.R.; Vilar, V.J.P. Assessment of AOPs as a polishing step in the decolourisation of bio-treated textile wastewater: Technical and economic considerations. *J. Photochem. Photobiol. A Chem.* **2016**, *317*, 26–38. [CrossRef]
15. Al-Mamun, M.R.; Kader, S.; Islam, M.S.; Khan, M.Z.H. Photocatalytic activity improvement and application of UV-TiO_2 photocatalysis in textile wastewater treatment: A review. *J. Environ. Chem. Eng.* **2019**, *7*, 103248. [CrossRef]
16. Spasiano, D.; Marotta, R.; Malato, S.; Fernandez-Ibañez, P.; Di Somma, I. Solar photocatalysis: Materials, reactors, some commercial, and pre-industrialized applications. A comprehensive approach. *Appl. Catal. B Environ.* **2015**, *170*, 90–123. [CrossRef]
17. Marcelino, R.B.P.; Amorim, C.C. Towards visible-light photocatalysis for environmental applications: Band-gap engineering versus photons absorption—A review. *Environ. Sci. Pollut. Res.* **2019**, *26*, 4155–4170. [CrossRef]
18. Vaiano, V.; Iervolino, G. Photocatalytic removal of methyl orange azo dye with simultaneous hydrogen production using Ru-modified Zno photocatalyst. *Catalysts* **2019**, *9*, 964. [CrossRef]
19. AlSalka, Y.; Granone, L.I.; Ramadan, W.; Hakki, A.; Dillert, R.; Bahnemann, D.W. Iron-based photocatalytic and photoelectrocatalytic nano-structures: Facts, perspectives, and expectations. *Appl. Catal. B Environ.* **2019**, *244*, 1065–1095. [CrossRef]
20. Montenegro-Ayo, R.; Morales-Gomero, J.C.; Alarcon, H.; Cotillas, S.; Westerho, P.; Garcia-segura, S. Scaling up photoelectrocatalytic Reactors: A TiO_2 nanotube-coated disc compound reactor effectively degrades acetaminophen. *Water* **2019**, *11*, 2522. [CrossRef]
21. Deng, F.; Zhang, Q.; Yang, L.; Luo, X.; Wang, A.; Luo, S.; Dionysiou, D.D. Visible-light-responsive graphene-functionalized Bi-bridge Z-scheme black BiOCl/Bi_2O_3 heterojunction with oxygen vacancy and multiple charge transfer channels for efficient photocatalytic degradation of 2-nitrophenol and industrial wastewater treatment. *Appl. Catal. B Environ.* **2018**, *238*, 61–69. [CrossRef]
22. Tugaoen, H.O.N.; Garcia-Segura, S.; Hristovski, K.; Westerhoff, P. Compact light-emitting diode optical fiber immobilized TiO_2 reactor for photocatalytic water treatment. *Sci. Total Environ.* **2018**, *613*, 1331–1338. [CrossRef] [PubMed]
23. Fagan, R.; Mccormack, D.E.; Dionysiou, D.D.; Pillai, S.C. A review of solar and visible light active TiO_2 photocatalysis for treating bacteria, cyanotoxins and contaminants of emerging concern. *Mater. Sci. Semicond. Process.* **2016**, *42*, 2–14. [CrossRef]
24. Batista, L.M.B.; dos Santos, A.J.; da Silva, D.R.; Alves, A.P.D.M.; Garcia-Segura, S.; Martínez-Huitle, C.A. Solar photocatalytic application of NbO_2OH as alternative photocatalyst for water treatment. *Sci. Total Environ.* **2017**, *596*, 79–86. [CrossRef] [PubMed]
25. Dominguez, S.; Huebra, M.; Han, C.; Campo, P.; Nadagouda, M.N.; Rivero, M.J.; Ortiz, I.; Dionysiou, D. Magnetically recoverable TiO_2-WO_3 photocatalyst to oxidize bisphenol A from model wastewater under simulated solar light. *Environ. Sci. Pollut. Res.* **2017**, *24*, 12589–12598. [CrossRef] [PubMed]
26. Zuorro, A.; Lavecchia, R.; Monaco, M.M.; Iervolino, G.; Vaiano, V. Photocatalytic degradation of azo dye Reactive Violet 5 on Fe-doped Titania catalysts under visible light irradiation. *Catalysts* **2019**, *9*, 645. [CrossRef]
27. Idrees, F.; Dillert, R.; Bahnemann, D.; Butt, F.K.; Tahir, M. In-situ synthesis of Nb_2O_5/g-C_3N_4 heterostructures as highly efficient photocatalysts for molecular h2 evolution under solar illumination. *Catalysts* **2019**, *9*, 169. [CrossRef]
28. Prado, A.G.S.; Bolzon, L.B.; Pedroso, C.P.; Moura, A.O.; Costa, L.L. Nb_2O_5 as efficient and recyclable photocatalyst for indigo carmine degradation. *Appl. Catal. B Environ.* **2008**, *82*, 219–224. [CrossRef]
29. Leite, E.R.; Vila, C.; Bettini, J.; Longo, E. Synthesis of niobia nanocrystals with controlled morphology. *J. Phys. Chem. B* **2006**, *110*, 18088–18090. [CrossRef]
30. Heitmann, A.P.; Patrício, P.S.O.; Coura, I.R.; Pedroso, E.F.; Souza, P.P.; Mansur, H.S.; Mansur, A.; Oliveira, L.C.A. Nanostructured niobium oxyhydroxide dispersed Poly (3-hydroxybutyrate) (PHB) films: Highly efficient photocatalysts for degradation methylene blue dye. *Appl. Catal. B Environ.* **2016**, *189*, 141–150. [CrossRef]
31. Aegerter, M.A. Sol-gel niobium pentoxide: A promising material for electrochromic coatings, batteries, nanocrystalline solar cells and catalysis. *Sol. Energy Mater. Sol. Cells* **2001**, *68*, 401–422. [CrossRef]

32. Wang, F.; Wu, H.Z.; Liu, C.L.; Yang, R.Z.; Dong, W.S. Catalytic dehydration of fructose to 5-hydroxymethylfurfural over Nb_2O_5 catalyst in organic solvent. *Carbohydr. Res.* **2013**, *368*, 78–83. [CrossRef] [PubMed]
33. Villaluz, F.J.A.; de Luna, M.D.G.; Colades, J.I.; Garcia-Segura, S.; Lu, M. Removal of 4-chlorophenol by visible-light photocatalysis using ammonium iron (II) sulfate-doped nano-titania. *Process Saf. Environ. Prot.* **2019**, *125*, 121–128.
34. Sathasivam, S.; Williamson, B.A.D.; Althabaiti, S.A.; Obaid, A.Y.; Basahel, S.N.; Mokhtar, M.; Scanlon, D.O.; Carmalt, C.; Parkin, I.P. Chemical vapor deposition synthesis and optical properties of Nb_2O_5 thin films with hybrid functional theoretical insight into the band structure and band gaps. *ACS Appl. Mater. Interfaces* **2017**, *9*, 18031–18038. [CrossRef]
35. Corrêa, M.D.P. Solar ultraviolet radiation: Properties, characteristics and amounts observed in Brazil and south America. *An. Bras. Dermatol.* **2015**, *90*, 297–313. [CrossRef]
36. Lin, J.C.; Sopajaree, K.; Jitjanesuwan, T.; Lu, M. Application of visible light on copper-doped titanium dioxide catalyzing degradation of chlorophenols. *Sep. Purif. Technol.* **2018**, *191*, 233–243. [CrossRef]
37. Anotai, J.; Jevprasesphant, A.; Lin, Y.M.; Lu, M.C. Oxidation of aniline by titanium dioxide activated with visible light. *Sep. Purif. Technol.* **2012**, *84*, 132–137. [CrossRef]
38. Brillas, E.; Garcia-Segura, S. Benchmarking recent advances and innovative technology approaches of Fenton, photo-Fenton, electro-Fenton, and related processes: A review on the relevance of phenol as model molecule. *Sep. Purif. Technol.* **2019**, 116337. [CrossRef]
39. Fujishima, A.; Zhang, X.; Tryk, D.A. TiO_2 photocatalysis and related surface phenomena. *Surf. Sci. Rep.* **2008**, *63*, 515–582. [CrossRef]
40. Hashemzadeh, F.; Rahimi, R.; Gaffarinejad, A. Influence of operational key parameters on the photocatalytic decolorization of Rhodamine B dye using $Fe^{2+}/H_2O_2/Nb_2O_5$/UV system. *Environ. Sci. Pollut. Res.* **2014**, *21*, 5121–5131. [CrossRef]
41. Venkatachalapathy, R.; Davila, G.P.; Prakash, J. Catalytic decomposition of hydrogen peroxide in alkaline solutions. *Electrochem. Commun.* **1999**, *1*, 614–617. [CrossRef]
42. Garcia-Segura, S.; Tugaoen, H.O.N.; Hristovski, K.; Westerhoff, P. Photon flux influence on photoelectrochemical water treatment. *Electrochem. Commun.* **2018**, *87*, 63–65. [CrossRef]
43. da Costa Filho, B.M.; Araujo, A.L.P.; Padrao, S.P.; Boaventura, R.A.R.; Dias, M.M.; Lopes, J.C.B.; Vilar, V.J.P. Effect of catalyst coated surface, illumination mechanism and light source in heterogeneous TiO_2 photocatalysis using a Mili-Photoreactor for n-Decane oxidation at gas phase. *Chem. Eng. J.* **2019**, *366*, 560–568. [CrossRef]
44. Heck, K.N.; Garcia-Segura, S.; Westerhoff, P.; Wong, M.S. Catalytic Converters for Water Treatment. *Acc. Chem. Res.* **2019**, *52*, 906–915. [CrossRef] [PubMed]
45. Nguyen, C.H.; Fu, C.C.; Juang, R.S. Degradation of methylene blue and methyl orange by palladium doped TiO_2 photocatalyst for water reuse: Efficiency and degradation pathways. *J. Clean Prod.* **2018**, *202*, 413–427. [CrossRef]
46. Wu, M.C.; Wu, P.Y.; Lin, T.H.; Lin, T.F. Photocatalytic performance of Cu-doped TiO_2 nanofibers treated by the hydrothermal synthesis and air-thermal treatment. *Appl. Surf. Sci.* **2018**, *430*, 390–398. [CrossRef]
47. Perillo, P.M.; Atia, M.N. Solar-assisted photodegradation of methyl orange using Cu-doped ZnO nanorods. *Mater. Today Commun.* **2018**, *17*, 252–258. [CrossRef]
48. Zheng, X.; Zhang, D.; Gao, Y.; Wu, Y.; Liu, Q.; Zhu, X. Synthesis and characterization of cubic Ag/TiO_2 nanocomposites for the photocatalytic degradation of methyl orange in aqueous solutions. *Inorg. Chem. Commun.* **2019**, *110*, 107589. [CrossRef]
49. Yin, H.; Zhou, A.; Chang, N.; Xu, X. Characterization and photocatalytic activity of Bi_3RiNbO_9 nanocrystallines synthesized by sol-gel process. *Mater. Res. Bull.* **2009**, *44*, 377–380. [CrossRef]
50. Tallapally, V.; Esteves, R.J.A.; Nahar, L.; Arachchige, U. Multivariate synthesis of tin phosphide nanoparticles: Temperature, time, and ligand control of size, shape, and crystal structure. *Chem. Mater.* **2016**, *28*, 5406–5414. [CrossRef]
51. Tallapally, V.; Damma, D.; Darmakkolla, S.R. Facile synthesis of size-tunable tin arsenide nanocrystals. *ChemmComm* **2019**, *55*, 1506–1563. [CrossRef] [PubMed]

52. Tallapally, V.; Nakagawara, T.A.; Demchenko, D.O.; Ozgur, U.; Arachchige, I.U. $Ge_{1-x}Sn_x$ alloy quantum dots with composition-tunable energy gaps and near-infrared photoluminescence. *Nanoscale* **2018**, *10*, 20296–20305. [CrossRef] [PubMed]
53. Dos Santos, A.J.; De Lima, M.D.; Da Silva, D.R.; Garcia-Segura, S.; Martínez-Huitle, C.A. Influence of the water hardness on the performance of electro-Fenton approach: Decolorization and mineralization of Eriochrome Black T. *Electrochim. Acta* **2016**, *208*, 156–163. [CrossRef]